iScience

CellPress
OPEN ACCESS

Article

# The compound packaged in virions is the key to trigger host glycolysis machinery for virus life cycle in the cytoplasm

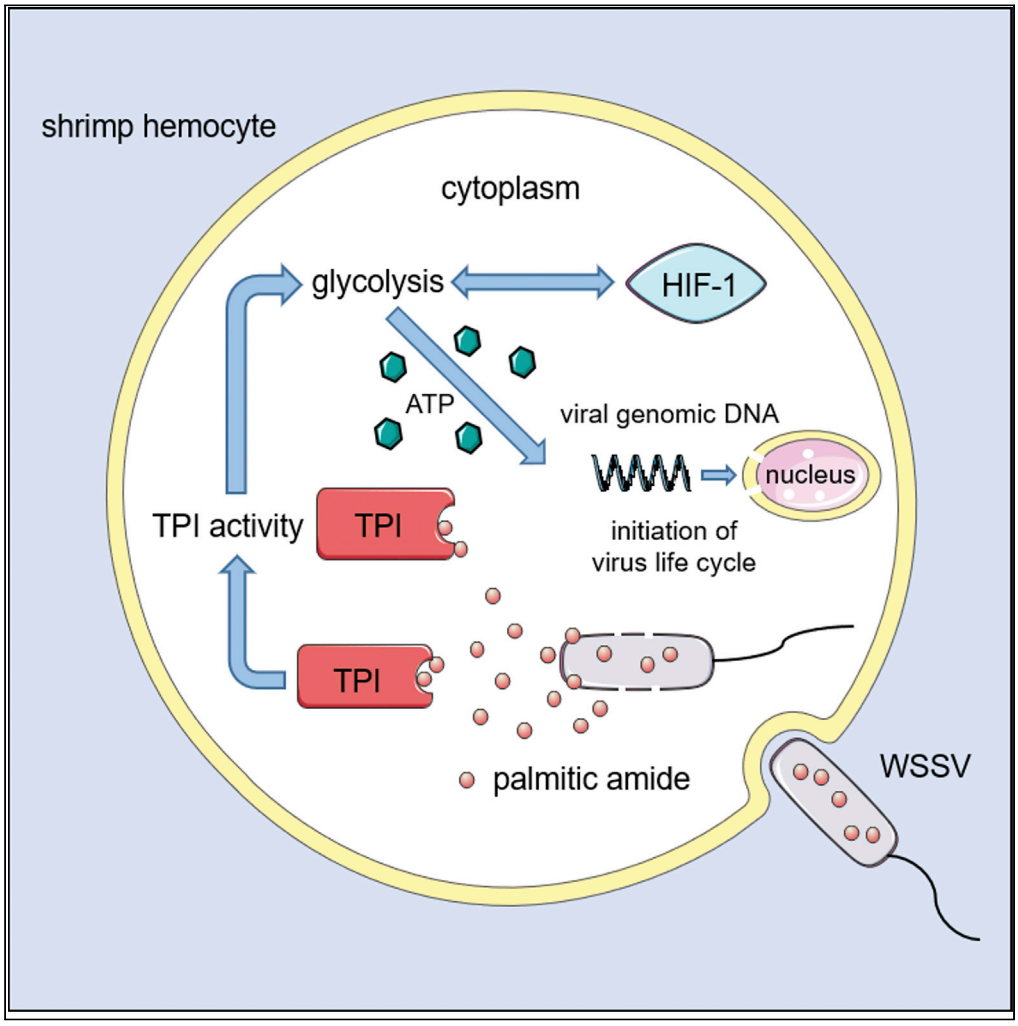


Siyuan Zhang, Fan Xin, Xiaobo Zhang

zxb0812@zju.edu.cn

## Highlights

Palmitic amide packaged in WSSV virions significantly promoted virus infection

Palmitic amide was released to upregulate HIF-1, leading to the enhanced glycolysis

Palmitic amide directly bound to TPI and promoted its activity

The enhanced TPI activity can upregulate glycolysis and the expression of HIF-1

Zhang et al., iScience *24*, 101915
January 22, 2021 
https://doi.org/10.1016/j.isci.2020.101915

iScience

CellPress
OPEN ACCESS

Article

# The compound packaged in virions is the key to trigger host glycolysis machinery for virus life cycle in the cytoplasm

Siyuan Zhang,[1] Fan Xin,[1] and Xiaobo Zhang[1,2,*]

## Summary

**Viruses depend on the host metabolic machinery to complete their life cycle in the host cytoplasm. However, the key viral factors initiating the host machinery after the virus enters the cytoplasm remain unclear. Here, we found that compounds packaged in the virions of white spot syndrome virus, such as palmitic amide, could trigger the viral life cycle in the host cytoplasm. Palmitic amide promoted virus infection by enhancing host glycolysis by binding to triosephosphate isomerase to enhance its enzymatic activity. The glycolysis enhancement resulted in lactate accumulation, thereby promoting hypoxia-inducible factor 1 (HIF-1) expression. HIF-1 upregulation further enhanced glycolysis, which in turn promoted virus infection. Therefore, our study presented novel insight into the initiation of the virus life cycle in host cells.**

## Introduction

Viruses are the most abundant life form on earth, inhabiting nearly every ecosystem, including animals, plants, bacteria, and environments. The entry of viruses into host cells is initiated by the recognition of receptors present on the surface of host cells (Sridharan et al., 2017). The receptors on the host cell membrane, the major mediators of virus tropism, interact with the viruses, leading to the occurrence of an apparently programmed series of molecular events to activate the receptors and the downstream pathways (Zhang et al., 2018). The binding of viral spikes to host cell surface receptors not only initiates viral adhesion and the engulfment process necessary for internalization but also can simultaneously initiate direct fusion with the cell membrane (Tsai et al., 2003). After interactions with host cell receptors, viruses enter host cells through either the endosomes or plasma membranes of host cells to undergo infection (Luo et al., 2018). Subsequently, both enveloped and nonenveloped viruses must deliver their genomes into host cells to initiate the virus life cycle in the host cells (Zhang et al., 2018). To move inside host cells, incoming viruses often exploit the cytoskeleton and cellular motor proteins of host cells (Hoffmann et al., 2017). The viruses allow endocytic vesicles to ferry them as passive lumenal cargo, or the penetrated capsid can itself interact with the relevant motors (Fernandez et al., 2019). Then, the viruses replicate within living cells and use the cellular machinery for the synthesis of their genomes and other components. However, it is not clear how the virus manipulates the host metabolic machinery to initiate virus infection in the host cytoplasm.

It is well known that all cells, whether differentiated or not, rely heavily on carbohydrate metabolism to create energy. Carbohydrate metabolism includes glycolysis in the cytoplasm and the tricarboxylic acid (TCA) cycle in mitochondria (Mizock, 1995; Vlashi et al., 2011). Glycolysis is a process whereby glucose is converted anaerobically into pyruvate by a series of intercellular enzymatic reactions to produce adenosine triphosphate (ATP), a high-energy phosphate compound (Noma, 1983; Schulze and Harris, 2012). In the presence of oxygen, cells yield two molecules of pyruvate, which are then converted to acetyl coenzyme A (acetyl CoA), triggering entry into the TCA cycle (Mizock, 1995; Hui et al., 2017). The TCA cycle is highly productive and efficient in terms of energy production (Noma, 1983; Hui et al., 2017). To ensure optimal environments for their replication and spread, viruses have evolved to alter the pathways of glycolysis, as well as glutaminolysis (Chambers et al., 2010). Most viruses examined to date induce aerobic glycolysis, also known as the Warburg effect (Chen et al., 2011). Many viruses can also induce fatty acid synthesis (Heaton and Randall, 2010). These modifications of carbon source utilization by viruses can increase the available energy for virus replication and virion production (Delgado et al., 2010). The expression of hexokinase 2, the first enzyme of glycolysis, is upregulated in dengue virus-infected cells (Fontaine et al., 2015).

[1]College of Life Sciences, Laboratory for Marine Biology and Biotechnology of Pilot National Laboratory for Marine Science and Technology (Qingdao) and Southern Marine Science and Engineering Guangdong Laboratory (Zhuhai), Zhejiang University, Hangzhou 310058, People's Republic of China

[2]Lead Contact

*Correspondence: zxb0812@zju.edu.cn

https://doi.org/10.1016/j.isci.2020.101915

Pharmacologically, inhibiting the glycolytic pathway dramatically reduces the RNA synthesis of dengue virus and the production of infectious virions, showing the requirement for glycolysis during dengue virus infection (Fontaine et al., 2015). Rhinovirus-infected cells rapidly upregulate glucose uptake in a PI3K-dependent manner, revealing a critical role of glucose mobilization from extracellular and intracellular pools via glycogenolysis for viral replication (Gualdoni et al., 2018). Viruses, as parasitic organisms, completely rely on host metabolic machinery for their survival. However, how viruses trigger host machinery to initiate the virus life cycle in the cytoplasm is unclear.

It is believed that viruses initiate their cellular infection by delivering their genomes, which are packaged in virions, into host cells. Except for viral genomes, however, it remains unknown whether any other molecules can be packaged in virions to manipulate virus infection. To explore whether there were any molecules, such as compounds, to be packaged in virions to initiate virus infection in the host cells, white spot syndrome virus (WSSV) was characterized in this study. WSSV, the type species of *Nimaviridae* family and *Whispovirus* genus, contains a circular double-stranded genomic DNA and has a wide range of hosts including shrimp, crab, and crayfish (Zhang et al., 2001; Cui et al., 2015). The results of this study revealed that compounds could be packaged in WSSV virions. The further analysis indicated that palmitic amide packaged in virions promoted virus infection by manipulating glycolysis of host cells.

## Results

### Metabolites packaged in virions

To explore the viral key to initiating host metabolic machinery, molecules packaged in virions, except for the viral genome, were characterized in this study. Virions of WSSV were purified from WSSV-challenged shrimp (Figure 1A). The liquid chromatography-coupled mass spectrometry (LC-MS) data of the metabolites extracted from the purified WSSV virions revealed a total of 1079 unique peaks, 9 of which were enriched in the WSSV virions compared with those in the control (Figure 1B). The nine peaks were identified as palmitic amide, sphinganine, linoleamide, oleamide, clusiacyclol A, myxochelin B, eplerenone, methionyl-leucylphenylalanine, and militarinone A. Therefore, the metabolites packaged in virions were further investigated.

At present, standards for the 4 compounds (palmitic amide, oleamide, linoleamide, and eplerenone) are available. To confirm the LC-MS data, therefore, the pure standards of palmitic amide, oleamide, linoleamide, and eplerenone were subjected to LC-MS analysis. The LC-MS peaks of palmitic amide and oleamide extracted from the WSSV virions matched those of their corresponding standards (Figure 1C), confirming the LC-MS data. However, the LC-MS peaks of linoleamide and eplerenone extracted from the WSSV virions did not match those of the standards (Figure 1C). These data showed that palmitic amide and oleamide (Figure 1D) were packaged in the WSSV virions.

### Effects of the metabolites packaged in virions on virus infection

To reveal the effects of palmitic amide and oleamide packaged in virions on virus infection, the compounds were injected into WSSV-infected shrimp, followed by the detection of WSSV infection. The LC-MS results indicated that the content of palmitic amide or oleamide in the shrimp hemocytes reached the highest point at 12 and 24 hr after compound injection, and the level of compounds dropped significantly 48 hr later (Figure 2A), indicating that the injected compound could maintain a high level in shrimp for at least 24 hr. The quantitative real-time polymerase chain reaction (PCR) data revealed that WSSV copies were significantly increased in shrimp treated with palmitic amide in a dose-dependent manner (Figure 2B). The optimal concentration of palmitic amide was 100 μM. However, oleamide had no effect on virus replication (Figure 2B). These results indicated that the palmitic amide packaged in the WSSV virions played a positive role in virus infection.

To explore the influence of the constant presence of palmitic amide in shrimp on virus infection, shrimp were injected with 100 μM palmitic amide first, and twenty four hours later, the same shrimp were injected with WSSV and palmitic amide (100 μM), followed by the injection of palmitic amide (100 μM) at 24 hr after WSSV infection. The results showed that the WSSV content in shrimp was much higher in shrimp treated with WSSV and palmitic amide than in shrimp treated with WSSV alone (Figure 2C). The shrimp mortality analysis yielded similar results (Figure 2D). However, the mortality of palmitic amide-treated shrimp was comparable to that of the negative controls (dimethyl sulfoxide [DMSO]) (Figure 2D), indicating that palmitic amide displayed no cytotoxicity to shrimp. These findings revealed that the metabolite palmitic amide packaged in virions could promote virus infection *in vivo*.

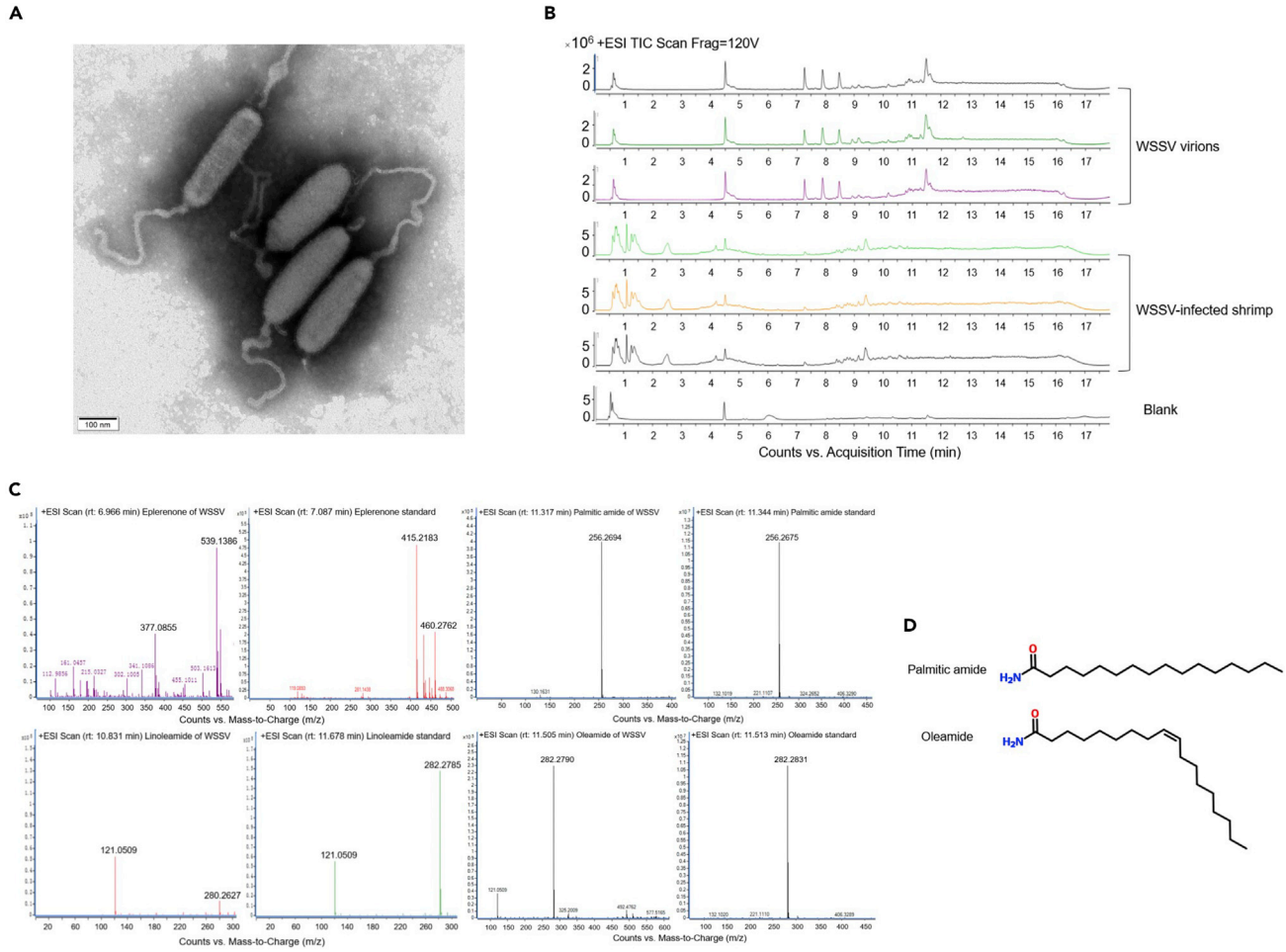


**Figure 1. Metabolites packaged in virions**

(A) WSSV virions purified from WSSV-infected shrimp. The purified virions were observed under a transmission electron microscope. Scale bar, 100 nm.

(B) LC-MS profiles of metabolites from the WSSV virions. The images were representatives of three biological repeats. The virus supernatant subjected to metabolite extraction and LC-MS analysis served as "blank".

(C) Confirmation of compounds packaged in WSSV virions by LC-MS analysis.

(D) Structures of palmitic amide and oleamide.

## Activation of the host HIF-1 signaling pathway and glycolysis by palmitic amide

To explore the effects of palmitic amide packaged in virions on host signaling pathways during virus infection, shrimp were injected with palmitic amide, followed by transcriptome analysis of shrimp hemocytes. After removal of repetitive and low-quality reads, a total of $5.04\times10^6$ high-quality reads were aligned to the assembled expressed sequence tags of shrimp. In total, 33,323 unigenes were obtained. Cluster analysis revealed that the pattern of mRNA expression levels in shrimp hemocytes was changed in response to palmitic amide treatment. Twelve genes were significantly upregulated and 26 genes were significantly downregulated compared with those in the control (Figure 3A). The upregulated genes included the metabolic activator hypoxia-inducible factor 1 (HIF-1), L-lactate dehydrogenase (LDH), and growth stimulator cyclin-dependent kinase 10 (CDK10), while the downregulated genes contained many genes, such as transcriptional coactivator YAP1, E3 ubiquitin-protein ligase RNF19A, and autophagy-related protein 5 (ATG5). To reveal the functions of these differentially expressed genes, Kyoto Encyclopedia of Genes and Genomes (KEGG) analysis was conducted. The results of KEGG analysis revealed that the differentially expressed genes were involved in signal transduction, gene transcription, cell growth and death, glycolysis, and other pathways (Figure 3B). To confirm the transcriptome analysis data, quantitative real-time PCR was conducted. The results showed that the genes encoding LDH, HIF-1, and CDK10 were upregulated, while the genes encoding ATG5, YAP1, and RNF19A were downregulated (Figure 3C), which were consistent with those of transcriptome sequencing, confirming the transcriptome

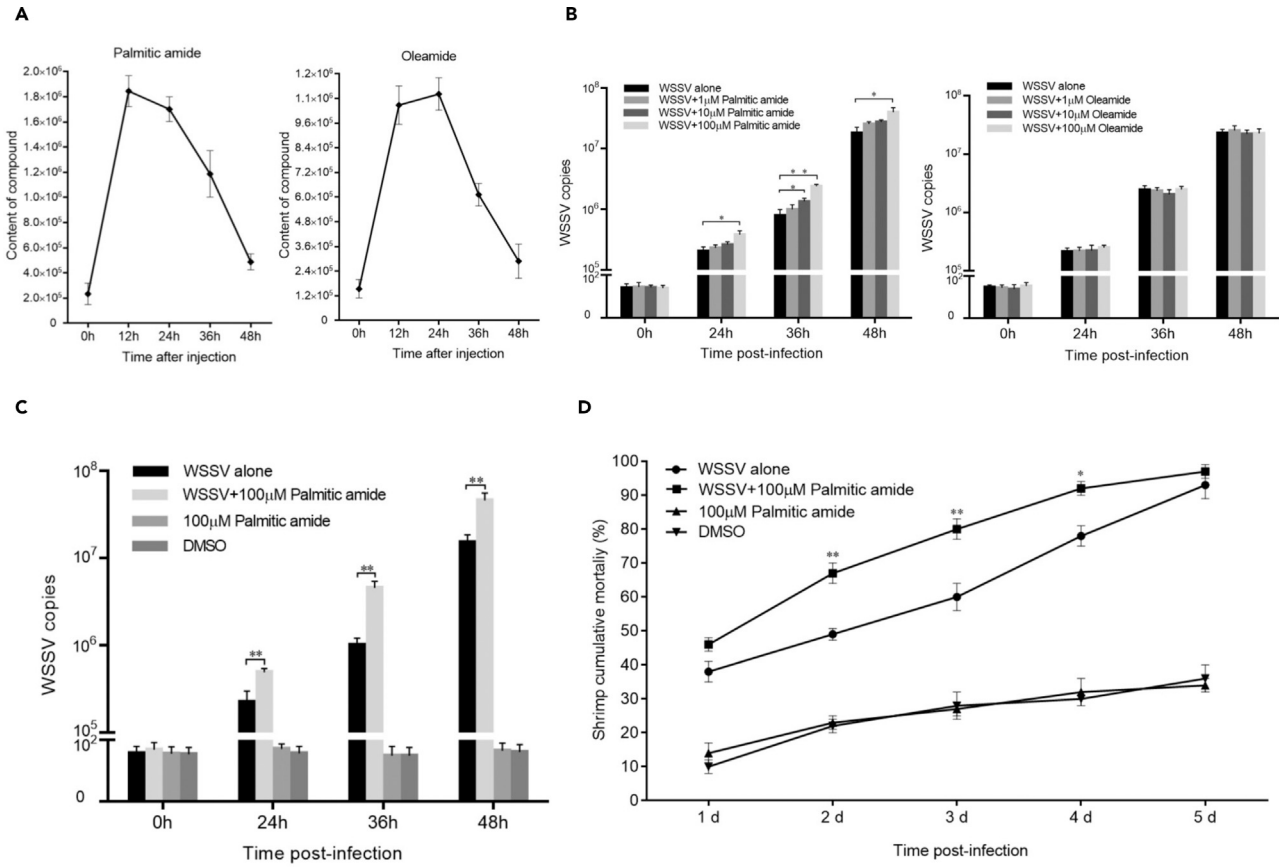


**Figure 2. Effects of the metabolites packaged in virions on virus infection**

(A) Content of compounds in shrimp hemocytes at different times after the injection of compounds. Palmitic amide and oleamide were injected into WSSV-infected shrimp. At different times after the compound injection, the content of compounds in the shrimp hemocytes was examined by LC-MS. The data represented the results of three independent assays.

(B) Influence of palmitic amide and oleamide on WSSV infection. The compounds at various concentrations were injected into the WSSV-infected shrimp. At different times post-infection, the shrimp were subjected to quantitative real-time PCR to quantify the WSSV copies in the shrimp hemocytes. The experiments were biologically repeated for three times (*$p < 0.05$; **$p < 0.01$).

(C) Impact of constant existence of palmitic amide on WSSV content in shrimp. Shrimp were injected with palmitic amide and/or WSSV. WSSV alone was used as a positive control. Palmitic amide (100 μM) and DMSO (dimethyl sulfoxide) without WSSV were included in the injections as negative controls. For the treatment WSSV+100 μM palmitic amide, shrimp were injected three times to ensure the constant presence of palmitic amide. Firstly, shrimp were injected with 100 μM of palmitic amide. Twenty four hours later, the same shrimp were injected with WSSV and palmitic amide (100 μM). Finally, the shrimp were injected with palmitic amide (100 μM) at 24 hr after infection. At different times post-infection, the WSSV copies were quantified by quantitative real-time PCR (**$p < 0.01$).

(D) Shrimp cumulative mortality analysis. The treatments were indicated on the top. The numbers on the horizontal axis represented the days post-infection. Data represented the mean ± standard deviation of triplicate assays (*$p < 0.05$; **$p < 0.01$).

sequencing results. These data indicated that palmitic amide promoted virus proliferation by upregulating the expression of host metabolism-associated genes. As reported, glycolysis of host cells is enhanced by virus infection (Chen et al., 2011; Fontaine et al., 2015), while HIF-1 is a key transcription factor regulating the glycolysis pathway (Yeung et al., 2008). In this context, HIF-1 was further characterized.

To investigate whether palmitic amide promoted virus infection through the HIF-1 signaling pathway, shrimp were injected with palmitic amide (100 μM), and then, the expression level of HIF-1 protein in hemocytes was examined. Western blot results showed that palmitic amide significantly upregulated the HIF-1 protein (Figure 3D), indicating that palmitic amide promoted the expression of HIF-1.

To evaluate whether palmitic amide affected the glycolytic reaction of shrimp, shrimp were injected with palmitic amide, followed by the detection of the contents of glucose and lactate in the shrimp hemocytes.

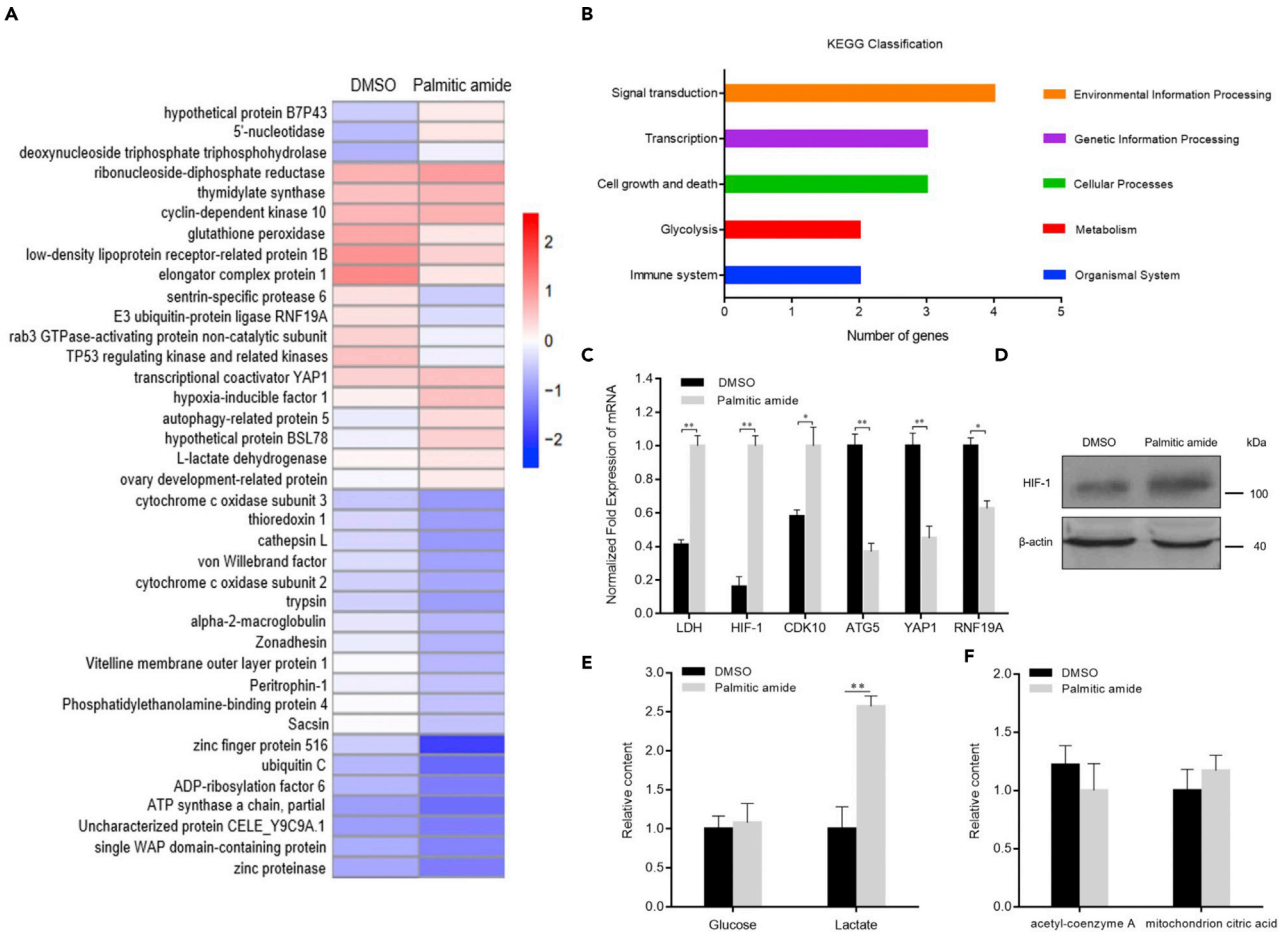


**Figure 3. Activation of the host HIF-1 signaling pathway and glycolysis by palmitic amide**

(A) Heatmap of differentially expressed genes of shrimp in response to palmitic amide challenge. Shrimp were injected with DMSO or palmitic amide. Twenty-four hours later, the mRNAs of shrimp hemocytes were subjected to sequencing.

(B) KEGG classification of the differentially expressed genes.

(C) Examination of the mRNA level of differentially expressed genes by quantitative real-time PCR. The error bars represent the means ± standard deviations of three independent experiments (*$p < 0.05$; **$p < 0.01$).

(D) Influence of palmitic amide on the expression of HIF-1. Shrimp were injected with DMSO or palmitic amide. Twenty-four hours later, Western blot analysis was conducted to examine the expression level of HIF-1 in shrimp hemocytes. β-actin was used as a control.

(E) Impact of palmitic amide on glycolysis of shrimp. Shrimp were injected with palmitic amide. As a control, DMSO was included in the injection. At 24 hr after injection, the contents of glucose and lactate in the hemocytes of shrimp were examined. The error bars represented the means ± standard deviations of three independent experiments (**$p < 0.01$).

(F) Role of palmitic amide in TCA cycle. Shrimp were injected with palmitic amide or DMSO. At 24 hr after injection, the contents of acetyl CoA and mitochondrial citric acid in the hemocytes of shrimp were examined.

The results showed that the lactate content was significantly increased in the palmitic amide-treated shrimp hemocytes compared with that in the controls, but the glucose content was unchanged (Figure 3E), indicating that palmitic amide promoted glycolysis of shrimp. At the same time, examination of the content of acetyl CoA and mitochondrial citric acid showed that palmitic amide had no effect on the host's TCA cycle (Figure 3F). The collective data demonstrated that when the virions entered the hemocytes, palmitic amide packaged in the virions was released to upregulate HIF-1, leading to the enhancement of glycolysis, and thus promoting virus infection.

## Role of HIF-1 in virus infection and glycolysis

To evaluate the role of shrimp HIF-1 in virus infection, the expression level of HIF-1 was examined in shrimp in response to WSSV challenge. The results indicated that HIF-1 was significantly upregulated in virus-challenged shrimp (Figure 4A), suggesting that HIF-1 was involved in virus infection. To explore the impact of

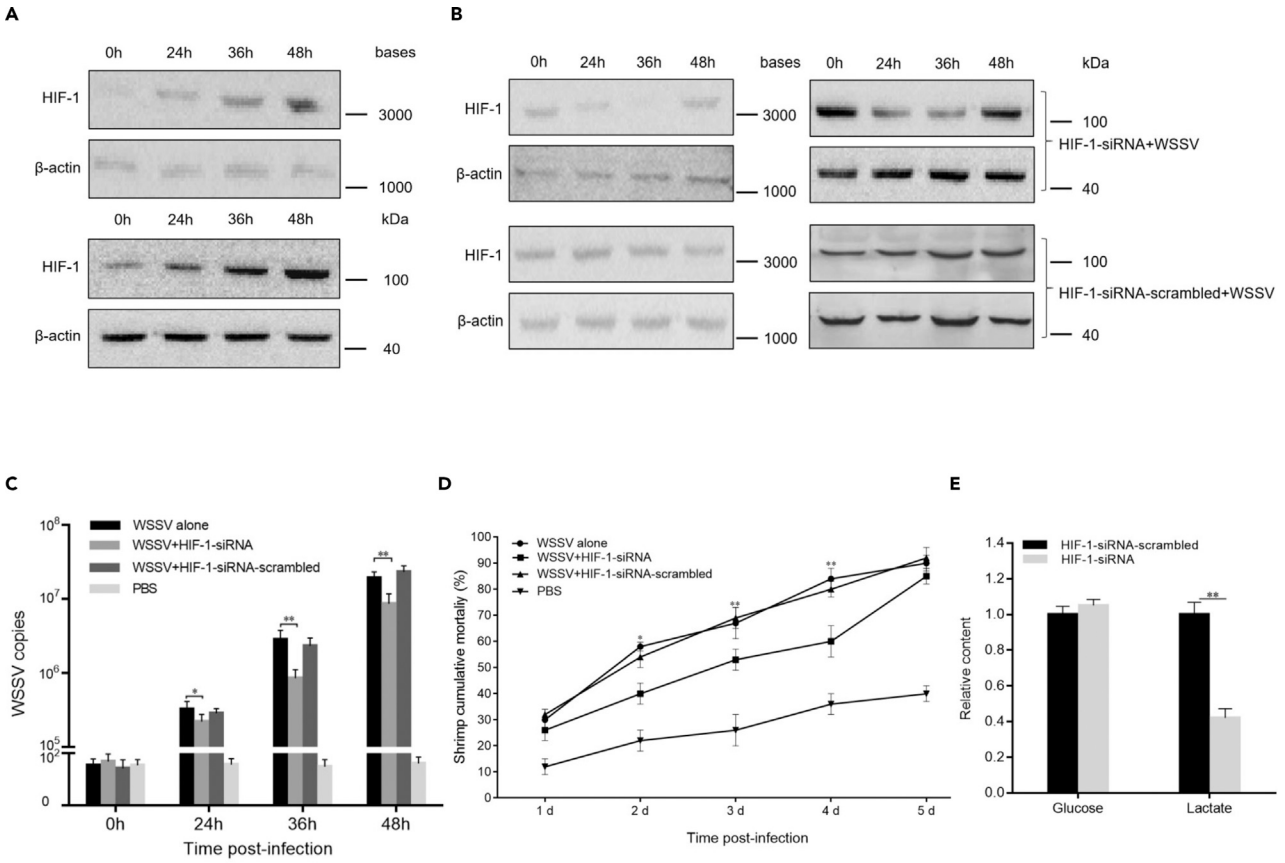


**Figure 4. Role of HIF-1 in virus infection and glycolysis**

(A) Upregulation of HIF-1 in shrimp in response to virus infection. Shrimp were challenged with WSSV. At different times post-infection, the expression level of HIF-1 in shrimp hemocytes was examined by Northern blot (up) and Western blot (down). β-actin was used as a control.

(B) Knockdown of HIF-1 by sequence-specific siRNA (HIF-1-siRNA) in WSSV-infected shrimp. Shrimp were co-injected with HIF-1-siRNA and WSSV. As a control, HIF-1-siRNA-scrambled was included in the injection. At different times after injection, the HIF-1 mRNA level and protein level in the hemocytes of shrimp were examined by Northern blot (left) and Western blot (right) separately. β-actin was used as a control.

(C) Influence of HIF-1 silencing on WSSV infection in shrimp. The WSSV content was quantified using quantitative real-time PCR at different times post-infection. WSSV alone, PBS, and HIF-1-scrambled were used as controls (*$p < 0.05$; **$p < 0.01$).

(D) Effects of HIF-1 silencing on the mortality of WSSV-infected shrimp. The numbers on the horizontal axis indicated the days post-infection (*$p < 0.05$; **$p < 0.01$).

(E) Role of HIF-1 in glycolysis of shrimp. Shrimp were injected with HIF-1-siRNA. HIF-1-siRNA-scrambled was included in the injection as a control. Thirty-six hours later, the contents of glucose and lactate in the hemocytes of shrimp were examined (**$p < 0.01$).

HIF-1 on virus infection, HIF-1 expression was knocked down by sequence-specific siRNA (HIF-1-siRNA) in shrimp (Figure 4B). The results revealed that HIF-1 silencing resulted in significant decreases in WSSV copies (Figure 4C). The mortality of WSSV-infected shrimp with HIF-1-siRNA treatment was also significantly decreased compared with that of the controls (Figure 4D). These data indicated that HIF-1 played a positive role in WSSV infection.

To explore whether HIF-1 affected the glycolytic reaction of shrimp, shrimp were injected with HIF-1-siRNA, and then, the contents of glucose and lactate in the hemocytes of shrimp were determined. The results showed that the lactate content was significantly decreased in HIF-1-siRNA-treated shrimp hemocytes compared with that in the controls, while the glucose content was not changed (Figure 4E), indicating that HIF-1 promoted glycolysis in shrimp.

## Palmitic amide interacted with the TPI protein and increased the TPI activity

To reveal the role of palmitic amide in the initiation of virus infection in host cells, the host proteins bound to palmitic amide were characterized. The results showed that a protein specifically bound to

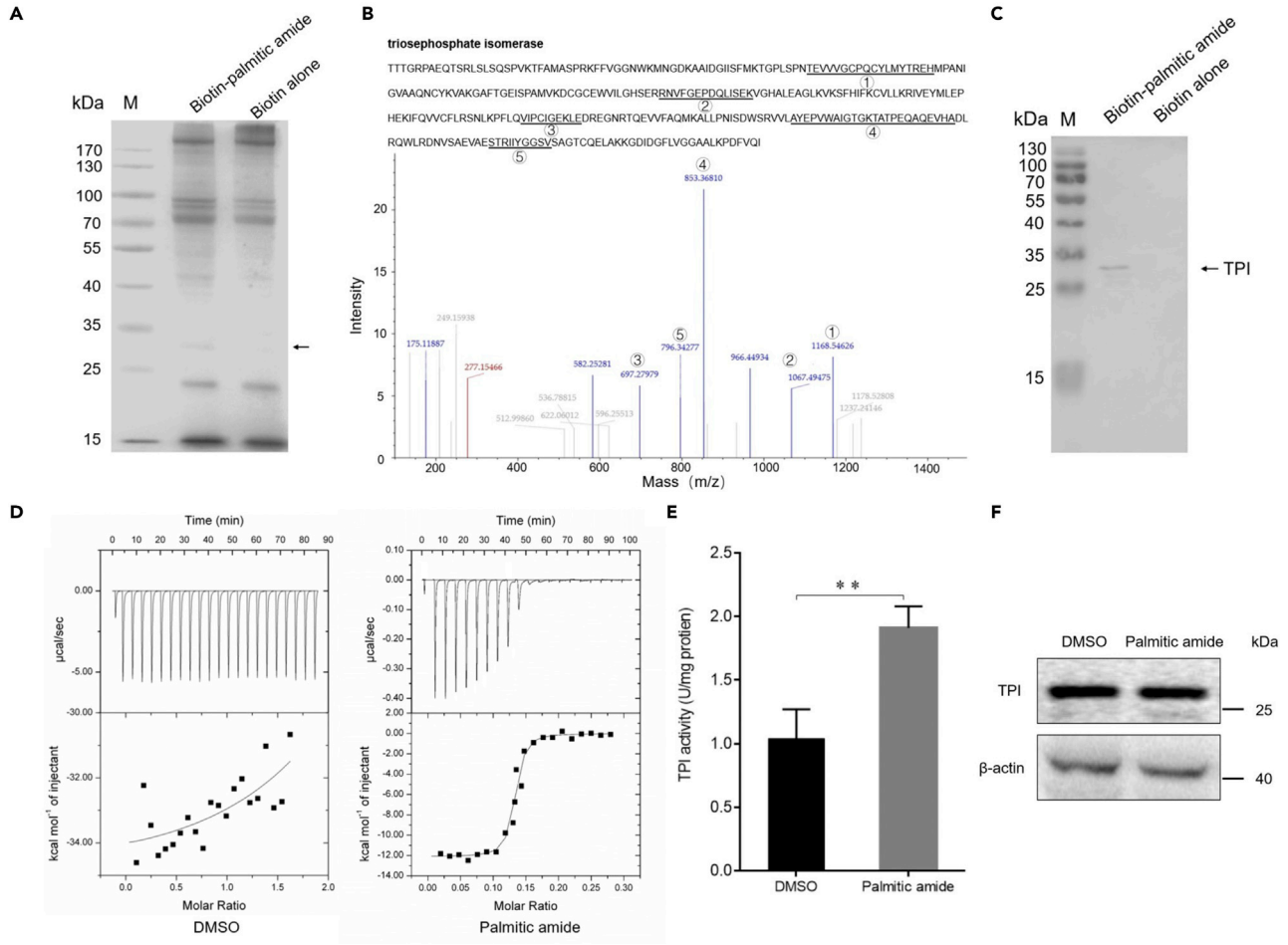


**Figure 5. Palmitic amide interacted with the TPI protein and increased the TPI activity**

(A) Proteins interacted with palmitic amide. Shrimp hemocytes were lysed and then incubated with biotin-labeled palmitic amide. The proteins were analyzed by SDS-PAGE with Coomassie blue staining. Dynabeads alone was used as a control. The arrow indicated the differential protein. M, protein marker.

(B) Identification of the protein bound to palmitic amide by mass spectrometry. The protein was identified to be triosephosphate isomerase. The matched peptides were indicated with underlines and numbers.

(C) Western blot analysis of the proteins interacted with palmitic amide. The arrow indicated the TPI. M, protein marker.

(D) Thermodynamic characterization of the interaction between palmitic amide and TPI protein. The purified recombinant TPI protein (100 μM) and incubated with palmitic amide (1 mM), followed by isothermal titration calorimetry (ITC) analysis. DMSO was used as a control.

(E) Impact of palmitic amide on TPI activity in shrimp. Shrimp were injected with palmitic amide (100 μM). Twenty-four hours later, the activity of TPI of hemocytes was examined. DMSO was used as a control. The error bars denoted the means ± standard deviations of three independent experiments (**$p < 0.01$).

(F) Influence of palmitic amide on the expression of TPI in shrimp. Shrimp were injected with palmitic amide (100 μM) or DMSO. Twenty-four hours later, the expression level of TPI in the hemocytes of shrimp was examined by Western blot analysis. β-actin was used as a control.

palmitic amide (Figure 5A). The protein was identified as triosephosphate isomerase (TPI) by mass spectrometry (Figure 5B). Western blot analysis confirmed the mass spectrometric data (Figure 5C). To characterize the direct interaction between palmitic amide and TPI, isothermal titration calorimetry analysis was conducted. The results indicated that the dissociation constant (Kd) of the binding of palmitic amide to the recombinant TPI protein was 4.89 ± 1.23 μM, while the Kd of the binding of DMSO to TPI protein was 0 (Figure 5D). These data showed that palmitic amide was directly bound to the TPI protein.

To evaluate the effects of palmitic amide on TPI activity, shrimp were injected with palmitic amide, followed by the detection of TPI enzymatic activity of hemocytes. The results showed that palmitic amide

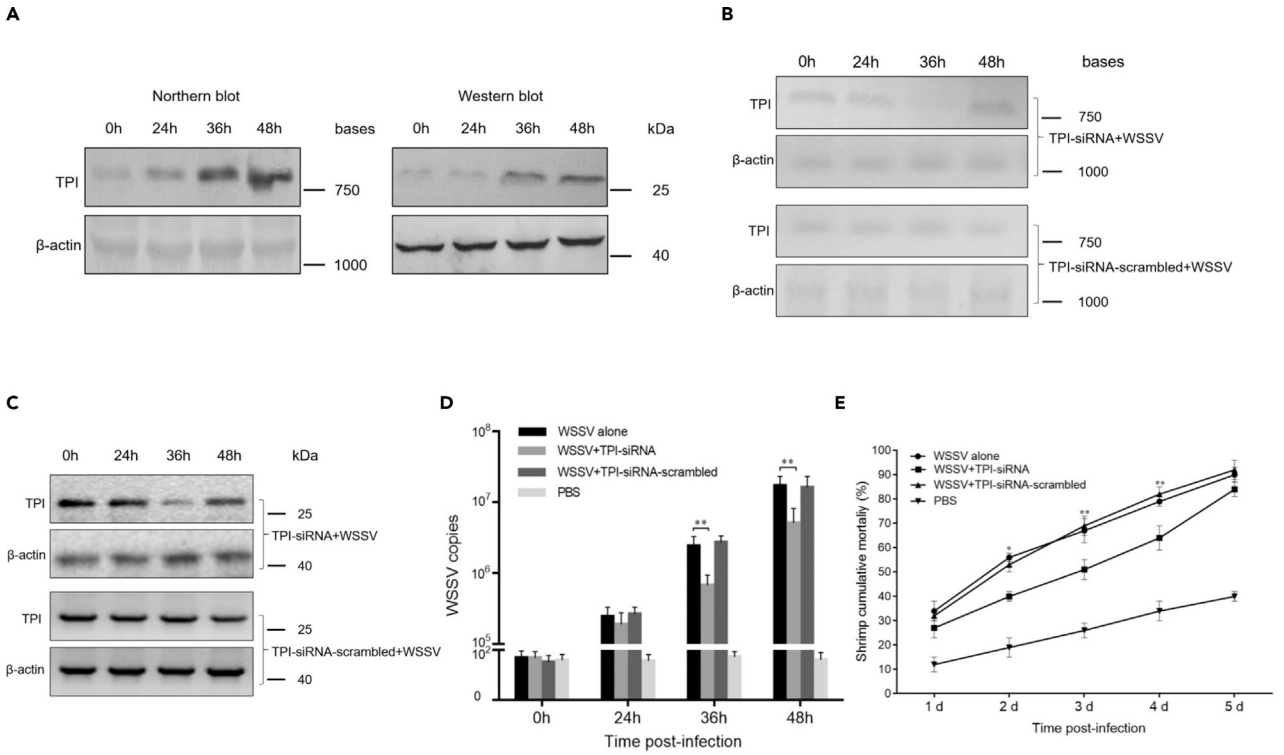


**Figure 6. The influence of TPI on virus infection**

(A) Upregulation of TPI in shrimp in response to virus infection. Shrimp were challenged with WSSV. At different times post-infection, the expression level of TPI in shrimp hemocytes was examined by Northern blot and Western blot. β-actin was used as a control.

(B) Knockdown of TPI by sequence-specific siRNA (TPI-siRNA) in WSSV-infected shrimp. Shrimp were co-injected with TPI-siRNA and WSSV. As a control, TPI-siRNA-scrambled was included in the injection. At different times after injection, the TPI mRNA level in the hemocytes of shrimp was examined by Northern blot. β-actin was used as a control.

(C) Western blot analysis of TPI protein in siRNA-treated shrimp. β-actin was used as a control.

(D) Influence of TPI silencing on WSSV infection in shrimp. The WSSV content was quantified using quantitative real-time PCR at different times post-infection. WSSV alone and PBS were used as controls. The error bars denoted the means ± standard deviations of three independent experiments (**$p < 0.01$).

(E) Effects of TPI silencing on the mortality of WSSV-infected shrimp. The numbers on the horizontal axis indicated the post-infection days (*$p < 0.05$; **$p < 0.01$).

treatment resulted in a significant increase in TPI activity compared with that in the control (Figure 5E), indicating that palmitic amide could enhance TPI activity. To assess whether palmitic amide affected the expression of TPI protein, the hemocytes of shrimp injected with palmitic amide were subjected to Western blot analysis. The results demonstrated that palmitic amide had no effect on the expression of TPI in shrimp compared with that in the controls (Figure 5F). These data indicated that the interaction between palmitic amide and TPI could increase TPI enzymatic activity but did not affect the expression level of TPI.

## The influence of TPI on virus infection

To explore the influence of TPI on virus infection, TPI expression in WSSV-infected shrimp was examined. The results indicated that TPI was upregulated in shrimp in response to virus challenge (Figure 6A). Western blot analysis yielded similar results (Figure 6A). These data demonstrated that TPI played an important role in virus infection. To reveal the role of TPI in virus infection, TPI was knocked down by sequence-specific TPI-siRNA in shrimp. Northern blot and Western blot data showed that TPI was silenced in WSSV-infected shrimp (Figures 6B and 6C). TPI silencing led to a significant decrease in WSSV content in shrimp (Figure 6D). However, TPI-siRNA scrambled had no effect on virus replication (Figure 6D). The mortality of WSSV-infected shrimp treated with TPI-siRNA was significantly decreased compared with that of the controls (Figure 6E). These data indicated that TPI played a positive role in WSSV infection.

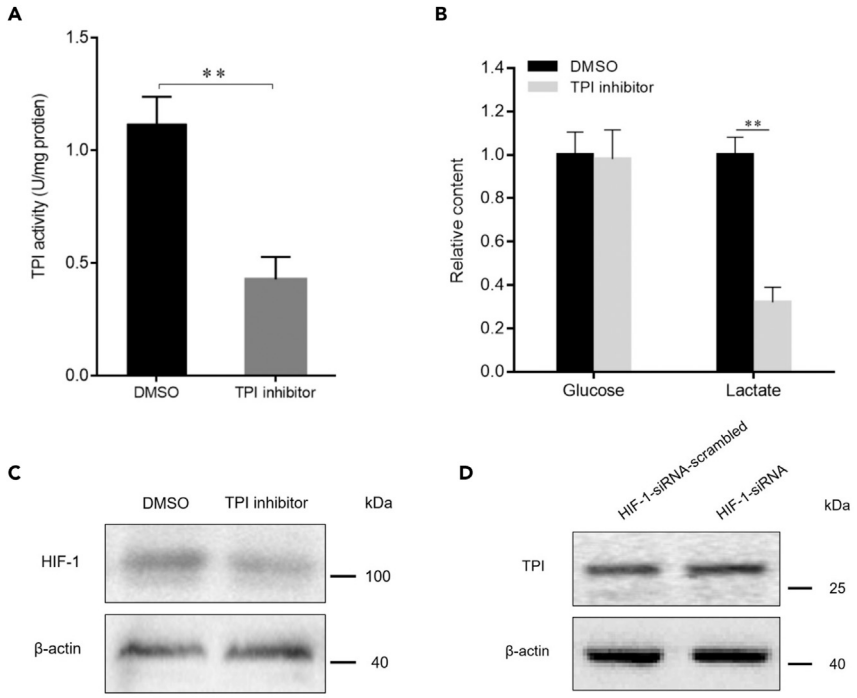


**Figure 7. Relationship between TPI, HIF-1, and glycolysis**

(A) Influence of TPI inhibitor on TPI activity in shrimp. Shrimp were injected with TPI inhibitor phenazine (100 μM). Twenty-four hours later, the enzymatic activity of TPI in the hemocytes of shrimp was examined. DMSO was used as a control. The error bars denoted the means ± standard deviations of three independent experiments (**$p < 0.01$).

(B) Impact of the inhibition of TPI activity on glycolysis of shrimp. At 24 hr after the injection of TPI inhibitor, the contents of glucose and lactate in the hemocytes of shrimp were examined. The error bars represented the means ± standard deviations of three independent experiments (**$p < 0.01$).

(C) Effects of the suppression of TPI activity on the HIF-1 expression in shrimp. At 24 hr after the injection of TPI inhibitor, Western blot analysis was conducted to examine the expression level of HIF-1 protein in shrimp hemocytes. β-actin was used as a control.

(D) Evaluation of the impact of HIF-1 silencing on the expression of TPI in shrimp. Shrimp were injected with HIF-1-siRNA. As a control, HIF-1-siRNA-scrambled was included in the injection. At 36 hr after injection, the expression level of TPI protein in the hemocytes of shrimp was analyzed by Western blot. β-actin was used as a control.

## Relationship between TPI, HIF-1, and glycolysis

To investigate the relationship between TPI, HIF-1, and glycolysis, shrimp were treated with the TPI enzyme-specific inhibitor (Alvarez et al., 2014), followed by analyses of HIF-1 expression and glycolysis. The results showed that the TPI-specific inhibitor significantly suppressed the enzymatic activity of TPI (Figure 7A). The suppression of TPI activity resulted in a significant decrease in lactate content (Figure 7B), showing that glycolysis was inhibited by a TPI-specific inhibitor. Western blot analysis indicated that the inhibition of TPI enzymatic activity significantly decreased HIF-1 protein levels (Figure 7C). These data demonstrated that the enhanced TPI enzyme activity could upregulate the expression of HIF-1 and promote glycolysis.

To evaluate the impact of HIF-1 on TPI expression, shrimp were injected with HIF-1-siRNA. Western blot results showed that the TPI protein level in the hemocytes of shrimp treated with HIF-1-siRNA did not change compared with that in the controls (treated with HIF-1-siRNA-scrambled) (Figure 7D), indicating that HIF-1 did not affect the expression of TPI protein.

## Mechanism of palmitic amide-triggered initiation of virus infection

Collectively, these findings revealed that when the virions invaded the host cells, the virions released packaged palmitic amide (Figure 8). Subsequently, palmitic amide directly bound to host TPI to enhance its enzymatic activity, thus enhancing host glycolysis in the cytoplasm (Figure 8). The enhancement of

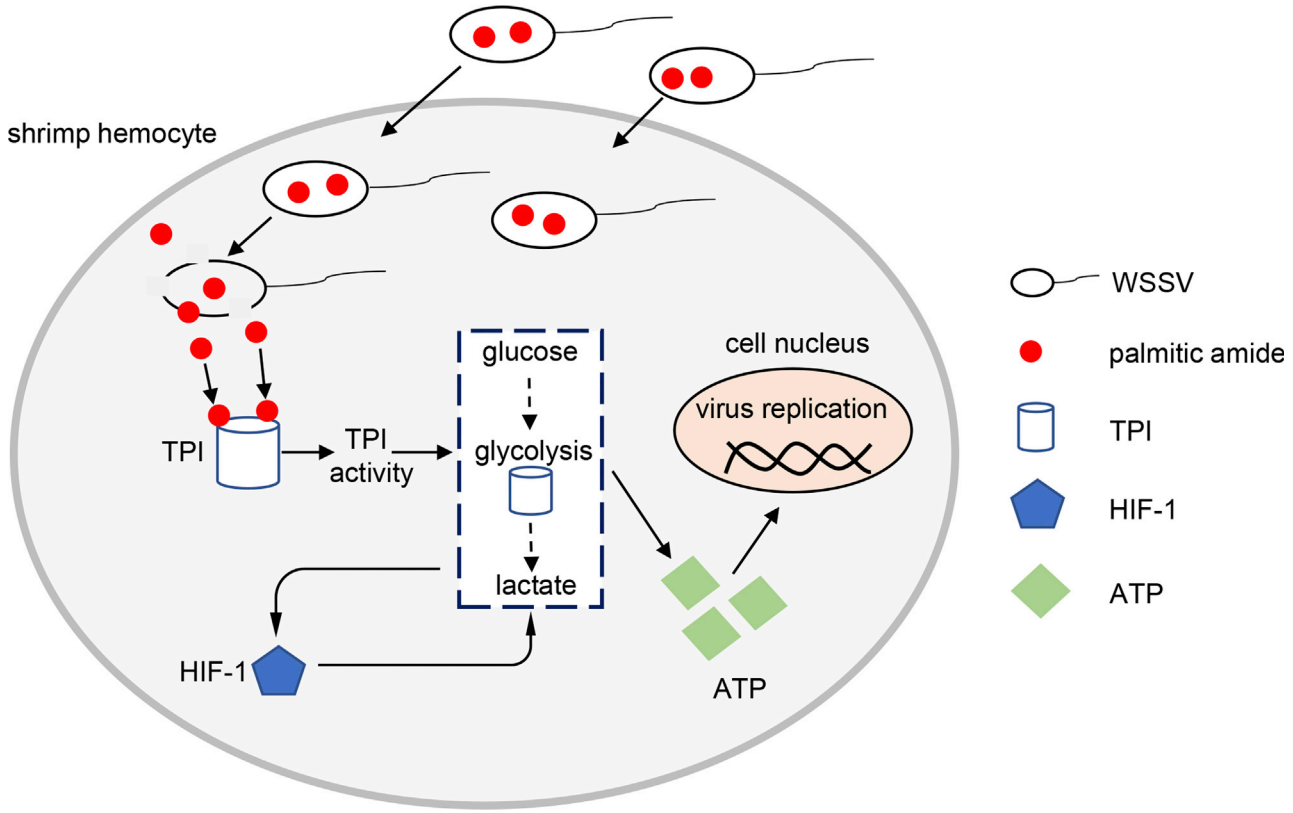


**Figure 8. Mechanism of palmitic amide-triggered initiation of virus infection**
Schematic diagram of the underlying mechanism of palmitic amide packaged in virions during virus infection.

glycolysis led to the accumulation of lactate in the cytoplasm, which entered the host cells into a hypoxic state, thereby promoting the expression of HIF-1 (Figure 8). The upregulated HIF-1 further promoted glycolysis (Figure 8). Therefore, the enhancement of glycolysis promoted virus infection (Figure 8).

## Discussion

Viruses initiate their life cycle and replicate within living cells by using the cellular machinery for the synthesis of their genomes and other components (Zhang et al., 2018). To gain access to host cells, viruses have evolved a variety of elegant mechanisms to utilize host energy. Following successful penetration into host cells, the virus particles need to reach an appropriate site in the cell for genome replication (Luo et al., 2018). The viral nucleocapsids are routed to the perinuclear area via microtubule-mediated transport. During this process, a dynein motor powers the movement of virus particles (Chou, 2007). For viruses that replicate in the nucleus, the viral genome needs to enter the nucleus via a nuclear pore (Smith and Helenius, 2004). Multiple distinct strategies are utilized, largely depending on the viral genome size (Schrad et al., 2020). Viral capsids of viruses with smaller genomes enter the nucleus, while for viruses with large genomes, the docking of nucleocapsids to a nuclear pore complex causes a partial disruption of the capsid or induces a minimal change in the viral capsid, allowing the transit of the DNA genome into the nucleus (Lakadamyali et al., 2003; Xie et al., 2019). At present, it is accepted that when a virus enters the cytoplasm of its host cell, the viral genome is released for gene expression and viral genome replication. However, there exists a gap between "after the virus enters the cytoplasm" and "before the virus initiates replication of the viral genome". It remains unclear how the virus initiates its life cycle in the host cytoplasm. Our findings revealed that compounds packaged in virions, such as palmitic amide, could initiate the virus life cycle by enhancing host glycolysis to provide energy for virus proliferation in the host cytoplasm. In this context, our study demonstrated novel insights into the initiation of the virus life cycle in host cells.

Glycolysis and the TCA cycle represent the two main metabolic pathways used to support the energetic needs of cells, which are the basis for all cellular activities (Pavlova and Thompson, 2016; Sanchez et al.,

2017). As reported, eukaryotic cells under normal growth conditions predominantly utilize glucose for oxidative phosphorylation in the mitochondria via the TCA cycle to generate the bulk of ATP (Janiszewska et al., 2012; Wang et al., 2019; Lebleu et al., 2014). In this study, however, the findings indicated that viruses initiate their life cycle by utilizing glycolysis but not the TCA cycle to support the energetic needs of virus proliferation in the cytoplasm of host cells. As well known, glycolysis is conducted in the cytoplasm, while the TCA cycle occurs in mitochondria. Therefore, it was easy for the compounds packaged in virions to utilize glycolysis in the cytoplasm without the entrance into mitochondria to trigger the TCA cycle. When the virus entered host cells, palmitic amide packaged in the virions was released to promote host glycolysis, thus initiating the virus life cycle. Although the production of lactic acid results in less ATP per molecule of glucose, it has been proposed that increased glycolysis and decreased oxidative phosphorylation may serve to increase the rate of ATP production without producing reactive oxygen species (Pinho and Reis, 2015; Courtnay et al., 2015), showing that energy is the first requirement for the initiation of virus infection in host cells. The large requirement of energy for virus restricted the energy supply for host cells, which might lead to host mortality. The compounds packaged in virions might be one of the important factors causing host mortality. Our study demonstrated that viruses could induce distinct alterations in host cellular metabolism to provide the energy and molecular building blocks needed for successful viral replication. In the initiation of the virus life cycle in host cells, the compounds packaged in virions played essential roles in manipulating the host's machinery for energy supply and could be the targets for therapy and diagnosis of virus-caused diseases. This issue merits to be explored in the future.

## Limitations of the study

For different viruses, the compounds packaged in virions may be different from each other. However, our study was limited to WSSV. It is unclear whether compounds packaged by other viruses interfere with host metabolism and affect viral infection.

## Resource availability

### *Lead contact*

Further information and requests for resources and reagents should be directed to and will be fulfilled by the Lead Contact, Xiaobo Zhang (zxb0812@zju.edu.cn).

### *Materials availability*

This study did not generate new unique reagents.

### *Data and code availability*

Original samples and data are available upon request.

## Methods

All methods can be found in the accompanying Transparent Methods supplemental file.

## Supplemental information

Supplemental Information can be found online at https://doi.org/10.1016/j.isci.2020.101915.

## Acknowledgments

This work was financially supported by the National Key Research and Development Program of China (2018YFD0900504) and China Ocean Mineral Resources R & D Association (DY135-B-04).

## Author contributions

X.Z. designed the experiments. S.Z. and X.F. conducted experiments and analyzed the data. S.Z. and X.Z. interpreted the results. S.Z. and X.Z. wrote the manuscript.

## Declaration of interests

All authors declare no competing interests.

Received: September 21, 2020
Revised: November 7, 2020
Accepted: December 4, 2020
Published: January 22, 2021

## References

Alvarez, G., Martinez, J., Aguirrelopez, B., Cabrera, N., Perezdiaz, L., de Gomez-Puyou, M.T., GómezPuyou, A., Pérez-Montfort, R., Garat, B., Merlino, A., et al. (2014). New chemotypes as Trypanosoma cruzi triosephosphate isomerase inhibitors: a deeper insight into the mechanism of inhibition. J. Enzyme Inhib. Med. Chem. *29*, 198–204.

Chambers, J.W., Maguire, T.G., and Alwine, J.C. (2010). Glutamine metabolism is essential for human cytomegalovirus infection. J. Virol. *84*, 1867–1873.

Chen, I.T., Aoki, T., Huang, Y.T., Hirono, I., Chen, T.C., Huang, J.Y., Chang, G.D., Lo, C.F., and Wang, H.C. (2011). White Spot Syndrome Virus induces metabolic changes resembling the Warburg effect in shrimp hemocytes in the early stage of infection. J. Virol. *85*, 12919–12928.

Chou, T. (2007). Stochastic entry of enveloped viruses: fusion versus endocytosis. Biophys. J. *93*, 1116–1123.

Cui, Y., Huang, T., and Zhang, X. (2015). RNA editing of microRNA prevents RNA-induced silencing complex recognition of target mRNA. Open Biol. *5*, 150126.

Courtnay, R., Ngo, D.C., Malik, N., Ververis, K., Tortorella, S.M., and Karagiannis, T.C. (2015). Cancer metabolism and the Warburg effect: the role of HIF-1 and PI3K. Mol. Biol. Rep. *42*, 841–851.

Delgado, T., Carroll, P.A., Punjabi, A.S., Margineantu, D., Hockenbery, D.M., and Lagunoff, M. (2010). Induction of the Warburg effect by Kaposi's sarcoma herpesvirus is required for the maintenance of latently infected endothelial cells. Proc. Natl. Acad. Sci. U S A *107*, 10696–10701.

Fernandez, J., Machado, A.K., Lyonnais, S., Chamontin, C., Gartner, K., Leger, T., Henriquet, C., Garcia, C., Portilho, D.M., Pugnière, M., et al. (2019). Transportin-1 binds to the HIV-1 capsid via a nuclear localization signal and triggers uncoating. Nat. Microbiol. *4*, 1840–1850.

Fontaine, K.A., Sanchez, E.L., Camarda, R., and Lagunoff, M. (2015). Dengue virus induces and requires glycolysis for optimal replication. J. Virol. *89*, 2358–2366.

Gualdoni, G.A., Mayer, K.A., Kapsch, A., Kreuzberg, K., Puck, A., Kienzl, P., Oberndorfer, F., Frühwirth, K., Winkler, S., Blaas, D., et al. (2018). Rhinovirus induces an anabolic reprogramming in host cell metabolism essential for viral replication. Proc. Natl. Acad. Sci. U S A *115*, 158–165.

Hoffmann, H.H., Schneider, W.M., Blomen, V.A., Scull, M.A., Hovnanian, A., Brummelkamp, T.R., and Rice, C.M. (2017). Diverse viruses require the calcium transporter SPCA1 for maturation and spread. Cell Host Microbe *22*, 460–470.

Hui, S., Ghergurovich, J.M., Morscher, R.J., Jang, C., Teng, X., Lu, W., Esparza, L.A., Reya, T., Zhan, L., Guo, J.Y., et al. (2017). Glucose feeds the TCA cycle via circulating lactate. Nature *551*, 115–118.

Heaton, N.S., and Randall, G. (2010). Dengue virus-induced autophagy regulates lipid metabolism. Cell Host Microbe *8*, 422–432.

Janiszewska, M., Suva, M.L., Riggi, N., Houtkooper, R.H., Auwerx, J., Clement-Schatlo, V., Radovanovic, I., Rheinbay, E., Provero, P., and Stamenkovic, I. (2012). Imp2 controls oxidative phosphorylation and is crucial for preserving glioblastoma cancer stem cells. Gene Dev. *26*, 1926–1944.

Luo, X., Yang, W., and Gao, G. (2018). SUN1 regulates HIV-1 nuclear import in a manner dependent on the interaction between the viral capsid and cellular cyclophilin A. J. Virol. *92*, e00229–18.

Lakadamyali, M., Rust, M.J., Babcock, H.P., and Zhuang, X. (2003). Visualizing infection of individual influenza viruses. Proc. Natl. Acad. Sci. U S A *100*, 9280–9285.

Lebleu, V.S., Oconnell, J.T., Herrera, K.N., Wikman, H., Pantel, K., Haigis, M.C., de Carvalho, F.M., Damascena, A., Chinen, L.T.D., Rocha, R.M., et al. (2014). PGC-1α mediates mitochondrial biogenesis and oxidative phosphorylation in cancer cells to promote metastasis. Nat. Cell Biol. *16*, 992–1003.

Mizock, B.A. (1995). Alterations in carbohydrate metabolism during stress: a review of the literature. Am. J. Med. *98*, 75–84.

Noma, A. (1983). ATP-regulated K+ channels in cardiac muscle. Nature *305*, 147–148.

Pinho, S.S., and Reis, C.A. (2015). Glycosylation in cancer: mechanisms and clinical implications. Nat. Rev. Cancer *15*, 540–555.

Pavlova, N.N., and Thompson, C.B. (2016). The emerging hallmarks of cancer metabolism. Cell Metab. *23*, 27–47.

Sridharan, H., Ragan, K.B., Guo, H., Gilley, R.P., Landsteiner, V.J., Kaiser, W.J., and Upton, J.W. (2017). Murine cytomegalovirus IE3-dependent transcription is required for DAI/ZBP1-mediated necroptosis. EMBO Rep. *18*, 1429–1441.

Sanchez, E.L., Pulliam, T., Dimaio, T.A., Thalhofer, A.B., Delgado, T., and Lagunoff, M. (2017). Glycolysis, glutaminolysis, and fatty acid synthesis are required for distinct stages of kaposi's sarcoma-associated herpesvirus lytic replication. J. Virol. *91*, e02237–16.

Smith, A.E., and Helenius, A. (2004). How viruses enter animal cells. Science *304*, 237–242.

Schulze, A., and Harris, A.L. (2012). How cancer metabolism is tuned for proliferation and vulnerable to disruption. Nature *491*, 364–373.

Schrad, J.R., Abrahão, J.S., Cortines, J.R., and Parent, K.N. (2020). Structural and proteomic characterization of the initiation of giant virus infection. Cell *181*, 1046–1061.

Tsai, B., Gilbert, J.M., Stehle, T., Lencer, W.I., Benjamin, T.L., and Rapoport, T.A. (2003). Gangliosides are receptors for murine polyoma virus and SV40. EMBO J. *22*, 4346–4355.

Vlashi, E., Lagadec, C., Vergnes, L., Matsutani, T., Masui, K., Poulou, M., Popescua, R., Donnaa, L.D., Eversa, P., Dekmeziana, C., et al. (2011). Metabolic state of glioma stem cells and nontumorigenic cells. Proc. Natl. Acad. Sci. U S A *108*, 16062–16067.

Wang, Z., Yip, L.Y., Lee, J.H., Wu, Z., Chew, H.Y., Chong, P.K., Teo, C.C., Ang, H.Y.K., Peh, K.L.E., Yuan, J., et al. (2019). Methionine is a metabolic dependency of tumor-initiating cells. Nat. Med. *25*, 825–837.

Xie, X., Zou, J., Zhang, X., Zhou, Y., Routh, A., Kang, C., Popov, V.L., Chen, X., Wang, Q.Y., Dong, H., and Shi, P.Y. (2019). Dengue NS2A protein orchestrates virus assembly. Cell Host Microbe *26*, 606–622.

Yeung, S.J., Pan, J., and Lee, M. (2008). Roles of p53, Myc and HIF-1 in regulating glycolysis - the seventh hallmark of cancer. Cell. Mol. Life Sci. *65*, 3981–3999.

Zhang, R., Kim, A.S., Fox, J.M., Nair, S., Basore, K., Klimstra, W.B., Rimkunas, R., Fong, R.H., Lin, H., Poddar, S., et al. (2018). Mxra8 is a receptor for multiple arthritogenic alphaviruses. Nature *557*, 570–574.

Zhang, X., Xu, X., and Hew, C.L. (2001). The structure and function of a gene encoding a basic peptide from prawn white spot syndrome virus. Virus Res. *79*, 137–144.

**iScience, Volume *24***

## Supplemental Information

# The compound packaged in virions is the key to trigger host glycolysis machinery for virus life cycle in the cytoplasm

**Siyuan Zhang, Fan Xin, and Xiaobo Zhang**

## Transparent Methods

### Shrimp culture and WSSV infection

*Marsupenaeus japonicus* shrimp with an average weight of 15 g, collected from a shrimp aquaculture farm at Hangzhou of Zhejiang province of China, were cultured in groups of 20 individuals in air-pumped circulating seawater at 25 ℃. Three shrimp were randomly selected for PCR detection of WSSV with WSSV-specific primers (5'-TTGGTTTCATGCCCGAGATT-3' and 5'-CCTTGGTCAGCCCCTTGA-3') to ensure that the shrimp used were WSSV free before experiments. The virus-free shrimp were infected with WSSV ($10^5$ copies/ml) by injection (100 μl WSSV inoculum/shrimp) into the lateral area of the fourth abdominal segment. At different times after infection, the WSSV-infected shrimp were collected for later use.

### Purification of intact WSSV virions

The tissues of WSSV-infected shrimp excluding hepatopancreas were collected in an ice-bathed beaker and then homogenized in 200 ml TNE buffer [50 mM Tris–HCl, 400 mM NaCl, 5 mM EDTA (ethylene diamine tetraacetic acid), pH 8.5] containing protease inhibitor phenylmethanesulfonyl fluoride. After centrifugation at 5,000×g for 10 min at 4 ℃, the supernatant was filtered through a nylon net (400 mesh). The filtrate was centrifuged at 30,000×g for 30 min at 4 ℃. Subsequently the upper loose pellet was rinsed out carefully, and the lower white pellet was resuspended in 50 ml TM buffer (50 mM Tris-HCl, 10 mM $MgCl_2$, pH 8.0). After centrifugation at 5,000×g for 10 min at 4 ℃, the virus particles were sedimented by centrifugation at 30,000×g

for 30 min, followed by resuspension with TM buffer. The purity of the virions was evaluated using negative-staining transmission electron microscopy (TEM).

**Metabolite analysis**

The WSSV-infected shrimp hemocytes or the purified WSSV virions ($10^{10}$ copies) were mixed with 99% methanol containing 0.05 mM 2-chloro-L-phenylalanine as an internal standard. The mixture was homogenized for 2 min and centrifuged at 12000×g at 4 ℃ for 10 min. Subsequently the supernatant (the extracted metabolites) was analyzed by liquid chromatography-coupled mass spectrometry (LC-MS) for metabolic profiling using Agilent 1290 Infinity II UHPLC system and Agilent 6545 UHD and Accurate-Mass Q-TOF/MS (Agilent Technologies, Santa Clara, CA, USA). The ESI-MS (electrospray ionization-mass spectrometry) was acquired in the positive ion mode. The product ions of m/z ranging from 50 to 1500 were collected. The heated capillary temperature was maintained at 325℃. The drying gas and nebulizer nitrogen gas flow rates were 10 L/min and 20 psi (pounds per square inch), respectively. The molecular feature extractor (MFE) algorithm within Mass Hunter Qualitative analysis software (Agilent Technologies, USA) was used to extract chemically qualified molecular features. For metabolite identification empirical formula generation, the molecular formula generator (MFG) algorithm was used to generate empirical formula and search against METLIN metabolite compound database (https://metlin.scripps.edu/) (Tautenhahn et al., 2012). Data processing was performed on each individual sample. The metabolite existed in all three samples of

each group was retained. According to the results of paired t-test analysis, the candidate differential metabolites were chosen according to the criteria ($p$<0.01 and fold change>3). To confirm the identified metabolites, pure standards of highest available purity (Sigma, USA) were prepared in 50% methanol. Then, the standard metabolite solution was analyzed with LC-MS. Matched retention time and mass spectral patterns of the standards and samples were compared.

**Effects of compounds on WSSV infection in shrimp**

WSSV ($10^5$ copies/ml) and the compound purchased from Sigma (USA) at different concentrations (1, 10 or 100 μM) were co-injected into virus-free shrimp at a volume of 100 μl per shrimp. The compounds were dissolved in dimethyl sulfoxide (DMSO). WSSV alone ($10^5$ copies/ml) and physiological saline (0.85% NaCl) were also injected into shrimp. At different times post-infection (0, 24, 36 and 48 h), three shrimp were randomly collected for each treatment and subjected to the detection of WSSV copies. The shrimp mortality was monitored every day. All assays were biologically repeated three times.

**Detection of WSSV copies by quantitative real-time PCR**

WSSV copies in shrimp were determined by quantitative real-time PCR as described before (Cui et al., 2015). DNA extracted from shrimp hemocytes was subjected to quantitative real-time PCR with WSSV-specific primers (5'-CCACCAATTCTACTCATGTACCAAA-3';
5'-TCCTTGCAATGGGCAAAATC-3') and probe

(5’-FAM-TGCTGCCGTCTCCAA-Eclipse-3’). A linearized plasmid containing a 1400-bp DNA fragment from the WSSV genome was quantified and serially diluted as an internal standard.

**Transcriptome sequencing**

A total of 1.5 μg RNA per sample was used for RNA sequencing. Sequencing libraries were generated using NEBNext® Ultra™ RNA Library Prep Kit for Illumina® (New England Biolabs, USA) following manufacturer’s recommendations and index codes were added to attribute sequences to each sample. Briefly, mRNA was purified from the total RNA using poly-T oligo-attached magnetic beads. Fragmentation was carried out using divalent cations under elevated temperature in NEB next first strand synthesis reaction buffer (5×). The first-stranded cDNA was synthesized with random hexamer primer and M-MuLV reverse transcriptase (RNase H). The second-stranded cDNA synthesis was subsequently performed using DNA polymerase I and RNase H. Remaining overhangs were converted into blunt ends via exonuclease/polymerase activities. After adenylation of 3’ ends of DNA fragments, NEB next adaptor with hairpin loop structure were ligated to prepare for hybridization. In order to select cDNA fragments of preferentially 250~300 bp in length, the library fragments were purified with AMPure XP system (Beckman Coulter, Beverly, USA). Then 3 μl USER enzymes (New England Biolabs) were used with size-selected adaptor-ligated cDNA at 37 °C for 15 min, followed by 5 min at 95 °C before PCR. PCR was performed with phusion high-fidelity DNA polymerase, universal PCR

primers and index primer. PCR products were purified (AMPure XP system) and library quality was assessed on the Agilent Bioanalyzer 2100 system.

**Kyoto encyclopedia of genes and genomes (KEGG) analysis**

The coding sequences of transcripts were extracted and used as queries to search the protein sequences collected in the GO (gene ontology) database with the blast E-value of less than $1\times10^{-5}$. The best hit GO identities were assigned to the transcripts. The p-values were corrected for false discovery rate. Deduced genes with homologues in other organisms were used to map to conserved biological pathways.

**Identification of proteins bound to palmitic amide**

To obtain the proteins interacted with palmitic amide, palmitic amide was labeled with biotin according to the manufacturer's instructions (Thermo Scientific, USA). Then the biotin-labeled palmitic amide was coupled to Dynabeads MyOne Streptavidin T1 (GE Healthcare, USA). Shrimp hemocytes were lysed with cell lysis buffer (20 mM Tris-HCl, 150 mM NaCl, 1% Triton X-100, pH 7.5) on ice for 2 h. After centrifugation at 15,000×g for 20 min, the supernatant was incubated with 1 mL of palmitic amide-coupled beads or negative control (Dynabeads alone) overnight at 4 °C with gentle rotation. The beads were washed five times with PBS to remove non-specific proteins. The mixture containing bound proteins was analyzed with SDS-PAGE. Proteins were visualized using Coomassie blue staining. The visible interested protein bands were excised from SDS-PAGE gel and subjected to protein identification by mass spectrometry (Bruker Daltonics, USA).

**RNAi (RNA interference) assay**

Small interfering RNA (siRNA) was designed and synthesized in vitro using a T7 kit according to the manufacturer's manual (TaKaRa, Japan). The siRNAs (TPI-siRNA, 5'-UGCUGACGAUCUUCUUGC-3'; TPI-siRNA-scrambled, 5'-CCAGCCU ACAAGAUUCCCAA-3'; HIF-1-siRNA, 5'-UACUAUCCUUCCCUGUACG-3'; HIF-1-siRNA-scrambled, 5'-AUGUACUGAGCUAAUUGCG-3') were dissolved in siRNA buffer (50 mM Tris-HCl, 100 mM NaCl, pH 7.5) and quantified by spectrophotometry. RNAi assay was conducted in shrimp by the injection of a siRNA (30 μg/shrimp) into the lateral area of the fourth abdominal segment using a syringe with a 29-gauge needle. At different times after injection, the shrimp hemocytes were collected for later use. The assays were biologically repeated for three times.

**Northern blotting**

Total RNAs were extracted using a mirVana miRNA isolation kit according to the manufacturer's instructions (Ambion, USA). Subsequently the total RNAs were electrophoresed in a denaturing 15% polyacrylamide gel containing 8 M urea and transferred to a Hybond-N membrane (Amersham Biosciences, Buckinghamshire, UK). After cross-linking with ultraviolet, the membrane was prehybridized in DIG (digoxigenin) Easy Hyb granule buffer (Roche, Switzerland) for 0.5 h, followed by hybridization with DIG-labeled TPI probe (5'-GGTCAGGCTCCCCGAAGAC-3') or HIF-1 probe (5'-CGAGGAGCGAAGATCTTGGATGTG-3') for 20 h at 45 ℃. Shrimp β-actin probe (5'-CTCGCTCGGCGGTGGTCGTGA-3') was included as a

control. Signal detection was performed following the instructions for a DIG High Prime DNA labeling and detection starter kit II (Roche, Switzerland).

**Isothermal titration calorimetry (ITC)**

The titration experiments were conducted on a VP-ITC platform (MicroCalTM, Inc., Northampton, MA, USA) at 25 °C to characterize the protein-compound interaction. The protein (at a final concentration of 100 μM) in the cell of the VP-ITC platform was added with a compound (1 mM) at 10 μL/120 s. All experiments were conducted at least in triplicate. The data were analyzed using Origin 7 and fitted to a "One-Sites" model (MicroCalTM Inc.). The thermodynamic association constant (Ka) and enthalpy change (ΔH) were calculated directly. The dissociation constant (Kd) was calculated according to the equation Kd = 1/Ka. The Gibbs free energy change (ΔG) was calculated using the equation $\Delta G = -RT\ln Ka$, where R was the molar gas constant and T was the absolute temperature at which the experiment was conducted. The entropy change (ΔS) of the interaction was calculated according to the equation $T\Delta S=\Delta H-\Delta G$.

**Examination of glycolysis**

To examine the shrimp glycolysis, shrimp hemocytes were collected, followed by the quantification of glucose and lactate contents. The hemocytes were centrifuged at 300×g for 10 min at 4 °C. Subsequently the concentration of glucose or lactate of the supernatant was determined using glucose assay kit (Beijing Solarbio Science & Technology Co., Ltd., China) or lactate assay kit (Solarbio, China). Briefly 20 μL of

sample was mixed with 200 μL of glucose or lactate working reagent in a single well of a 96-well plate. After incubation at 37 °C for 15 min for glucose or at 25 °C for 5 min for lactate, the absorbance of the sample was measured at 505 nm (glucose) or 570 nm (lactate). To quantify the content of glucose or lactate, a standard curve was generated. Subsequently the absolute content of glucose or lactate was determined.

**Western blot**

Proteins were separated using 12% SDS-PAGE and then transferred to a polyvinylidene fluoride (PVDF) membrane (Amersham Biosciences, UK). The membrane was blocked with TBST (Tris-buffered saline with Tween 20) containing 5% skimmed milk. Subsequently the membrane was incubated overnight with a primary antibody, followed by incubation with horseradish peroxidase (HRP)-conjugated secondary antibody (Sigma-Aldrich, USA) for 2 h at room temperature. The primary antibody was prepared in our laboratory. The proteins were detected using Western Lightning Plus-ECL Oxidizing Reagent Plus (PerkinElmer, USA).

**Detection of TPI enzymatic activity**

Cytoplasmic proteins were prepared using the NE-PER protein extraction kit (Pierce, Rockford, IL, USA). The protein concentration was measured with the Bradford protein assay (Bio-Rad Laboratories, Hercules, CA, USA). The enzymatic activity of TPI was determined as described previously (Olivaresillana et al., 2017), based on the conversion of glyceraldehyde 3-phosphate into dihydroxyacetone

phosphate 2. The cytoplasmic proteins (5 ng/mL) were mixed with the reaction buffer [100 mM triethanolamine, 10 mM ethylene diamine tetraacetic acid (EDTA), 0.2 mM nicotinamide adenine dinucleotide (NADH), 1 mM glyceraldehyde 3-phosphate (GAP) and 20 μg of α-glycerol phosphate dehydrogenase (α-GPDH)] at a final volume of 1 mL. After incubation at 25 °C for 5 min, the absorbance of the sample was measured at 340 nm with a plate reader. To quantify TPI enzymatic activity, a standard curve was generated. The TPI activity unit was determined as the micromoles of NADH formed per min per mg of protein at 25 °C.

**Examination of tricarboxylic acid cycle (TCA)**

To examine Sanchez the host's TCA, the contents of acetyl CoA and mitochondrial citric acid of hemocytes were measured using the acetyl CoA assay kit (Beijing Solarbio Science & Technology Co., Ltd., China) and the mitochondrial citric acid assay kit (Solarbio, China), respectively. Briefly 20 μL of sample was mixed with 200 μL of working reagent (Solarbio, China) in a single well of a 96-well plate. After incubation at 37 °C for 30 min, the absorbance of the sample was measured at 330 nm with a plate reader.

**Statistical analysis**

The numerical data from three independent experiments were analyzed by one-way analysis of variance (ANOVA). The differences between treatments were analyzed by Student's t-test.

**Supplemental References**

Cui, Y., Huang, T., & Zhang, X. (2015). RNA editing of microRNA prevents RNA-induced silencing complex recognition of target mRNA. Open Biol. 5 (12), 150126.

Olivaresillana, V., Riverosrosas, H., Cabrera, N., De Gomezpuyou, M. T., Perezmontfort, R., Costas, M., & Gomezpuyou, A. (2017). A guide to the effects of a large portion of the residues of triosephosphate isomerase on catalysis, stability, druggability, and human disease. Proteins 85 (7), 1190-1211.

Tautenhahn, R., Cho, K., Uritboonthai, W., Zhu, Z., Patti, G. J., & Siuzdak, G. (2012). An accelerated workflow for untargeted metabolomics using the METLIN database. Nat. Biotechnol. 30 (9), 826-828.